Journal of Materials Chemistry A

Facile synthesis and performances of nanosized Li2TiO3-based shell encapsulated LiMn1/3Ni1/3Co1/3O2 microsphere

Journal:	*Journal of Materials Chemistry A*
Manuscript ID:	TA-ART-02-2014-000888.R1
Article Type:	Paper
Date Submitted by the Author:	28-Mar-2014
Complete List of Authors:	yang, xiukang; Xiangtan University, School of Chemistry yu, ruizhi; Xiangtan University, School of Chemistry ge, long; Xiangtan University, shool of chemistry Xiangtan wang, di; Xiangtan University, School of Chemistry Zhao, Qinglan; Xiangtan university, school of chemistry wang, xianyou; Xiangtan University, shool of chemistry Bai, Yansong; Xiangtan University, shool of chemistry Xiangtan yuan, hao; xiangtan university, school of chemistry Shu, Hongbo; Xiangtan University, School of Chemistry

Journal Name ARTICLE

Cite this: DOI:

Facile synthesis and performances of nanosized Li_2TiO_3-based shell encapsulated $LiMn_{1/3}Ni_{1/3}Co_{1/3}O_2$ microsphere

Received
Accepted

DOI:

www.rsc.org/

Xiukang Yang, Ruizhi Yu, Long Ge, Di Wang, Qinglan Zhao, Xianyou Wang*, Yansong Bai, Hao Yuan, Hongbo Shu*

The $LiMn_{1/3}Ni_{1/3}Co_{1/3}O_2$ microsphere covered by nanosized Li_2TiO_3-based shell is prepared by a facile synthesis method. Controllable TiO_2 nano-layer growed firstly on the surface of spherical $Mn_{1/3}Ni_{1/3}Co_{1/3}CO_3$ precursor, and then the resultant TiO_2@$LiMn_{1/3}Ni_{1/3}Co_{1/3}O_2$ hybrid is synchronously transformed in situ into hierarchical Li_2TiO_3@$LiMn_{1/3}Ni_{1/3}Co_{1/3}O_2$ microsphere through solid phase reaction. It has been found that the hierarchical Li_2TiO_3@$LiMn_{1/3}Ni_{1/3}Co_{1/3}O_2$ microsphere exhibits a good rate capability with discharge capacity of 92.3 mAh g^{-1} even at high rate of 20 C between 3.0 and 4.3 V. Besides, it possesses excellent cyclic stability especially at high rate, with capacity retention of 90.3% after 500 cycles at 20 C rate. The enhanced electrochemical performance of the hierarchical Li_2TiO_3@$LiMn_{1/3}Ni_{1/3}Co_{1/3}O_2$ at high rate is attributed to the stable and fast Li^+-conductor characteristic of the nanosized Li_2TiO_3-based shell, thus the Li_2TiO_3@$LiMn_{1/3}Ni_{1/3}Co_{1/3}O_2$ microsphere will be a promising cathode material for power lithium ion batteries with high power density and excellent cycling performance.

Introduction

As an efficient energy storage and conversion system, rechargeable lithium ion batteries for use in small consumer devices have saturated society; however, if they are ever to be useful in large-scale applications such as electric vehicles (EV), hybrid electric vehicles (HEV), and utility powder grids, new attractive electrode materials with dramatically improved performance will be in urgent request.[1-4] Efforts to meet these objectives have initiated research into cathode materials with high power and energy densities, excellent stability, and low cost. In this respect, very appealing candidate is layered $LiMn_{1/3}Ni_{1/3}Co_{1/3}O_2$ oxide owing to its synergistic and favourable properties inherited from Ni-based, Co-based and Mn-based metal oxides.[5-10] Unfortunately, poor rate capability and inferior cyclic stability of the layered $LiMn_{1/3}Ni_{1/3}Co_{1/3}O_2$ cathode material are still the main problems in its high power and sustainability applications, which are mainly attributed to intrinsic low Li^+-ion conductivity of the materials and unstable Ni^{4+} and Co^{4+} ions when directly in contact with the electrolyte.

Various strategies have been attempted to deal with the above issues of the layered $LiMn_{1/3}Ni_{1/3}Co_{1/3}O_2$ oxide. One approach has been extensively adopted recently by integrating a structurally compatible component Li_2MnO_3 to stabilize $LiMn_{1/3}Ni_{1/3}Co_{1/3}O_2$ structure.[11,12] These materials are also regarded as solid solution between Li_2MnO_3 and $LiMn_{1/3}Ni_{1/3}Co_{1/3}O_2$ in the atomic level.[11] The Li_2MnO_3 component is of great significance because it can lend structural stability and provide additional high capacity to electrodes when electrochemically activated above 4.5 V. However, the activation of Li_2MnO_3 component will give rise to lattice breakdown and phase transformation (layered to spinel), resulting in poor rate capability and voltage fading of the materials during high voltage cycling.[13,14] Similar to Li_2MnO_3, Li_2TiO_3 is electrochemically inactive in a wide voltage range but strong Ti-O bond relative to Mn-O bond.[15-17] Besides, it has been demonstrated that the Li_2TiO_3 component is usually a fast Li^+-conductor when doping with other ions,[18,19] and can also stabilize the structure of layered electrodes without the risk of structural evolution like Li_2MnO_3-based materials.[20,21] Nevertheless, the Li_2TiO_3 component (including Li_2MnO_3) is usually distributed randomly throughout the composite structure, which can not provide an adequate protection to the active materials. Another effective method has involved the fabrication of "core-shell" architecture of the layered $LiMn_{1/3}Ni_{1/3}Co_{1/3}O_2$ by coating other media.[22-24] The coating shell can provide a complete shield in principle protecting against the dissolution of metal ions combined with a scavenging action for the fluoride anions eventually present in the electrolyte solution. However, these coating media are generally unfavourable for both Li^+-ion conduction of cathode materials and interfacial charge transfer of the electrode.[25,26] Furthermore, traditional coating methods, such as mechanical mixing and sol-gel, are usually divided into two steps: first synthesizing the cathode materials and second coating the active particles, which can not establish a controllable, uniform and complete coating shell on the core materials.[27,28] Therefore,

it is highly desirable to develop rational and controllable strategies for layered $LiMn_{1/3}Ni_{1/3}Co_{1/3}O_2$ with advanced architecture as well as good electrochemical performance.

Based on the above analysis, herein, we describe a facile synthesis method to in situ grow uniform Li_2TiO_3 nanosized-shell on the surface of $LiMn_{1/3}Ni_{1/3}Co_{1/3}O_2$ microsphere for the first time, and their formation of core-shell composite as advanced cathode material for lithium ion batteries. The effective method involves the growth of uniform TiO_2 nano-layer on the surface of spherical $Mn_{1/3}Ni_{1/3}Co_{1/3}CO_3$ precursor, and subsequent synchronous transition into hierarchical Li_2TiO_3@$LiMn_{1/3}Ni_{1/3}Co_{1/3}O_2$ through solid phase reaction. The unique hierarchical Li_2TiO_3@$LiMn_{1/3}Ni_{1/3}Co_{1/3}O_2$ microsphere with the advantages including 3D diffusion path for lithium ions and good structural stability as well as fast Li+ conductor characteristic of Li_2TiO_3-based shell, provides high rate capability and excellent cycling performance when evaluated as cathode material for lithium ion batteries.

Experimental

Synthesis of TiO_2@$Mn_{1/3}Ni_{1/3}Co_{1/3}CO_3$ microsphere

All reagents were of analytical grade and were purchased without further purification. $Mn_{1/3}Ni_{1/3}Co_{1/3}CO_3$ microsphere was firstly synthesized via co-precipitation of $MnSO_4{\cdot}H_2O$, $NiSO_4{\cdot}6H_2O$, and $CoSO_4{\cdot}7H_2O$ (1:1:1 in molar ratio) as starting materials. More details of the preparation procedures can be seen in our previous reports.[29,30] The obtained $Mn_{1/3}Ni_{1/3}Co_{1/3}CO_3$ microsphere was filtered, washed with deionized water, and then dried at 110 °C over night. A facile controllable method was carried out to grow TiO_2 nano-layer on the surface of $Mn_{1/3}Ni_{1/3}Co_{1/3}CO_3$ microsphere. The $Mn_{1/3}Ni_{1/3}Co_{1/3}CO_3$ microsphere (2.2 g) was dispersed in absolute ethanol (50 mL), and mixed with an appropriate amount of concentrated ammonia (25-28 wt %) under ultrasound for 30 min. In order to control the thickness and uniformity of TiO_2 shell, the amount of concentrated ammonia was varied in the range of 0-0.6 mL when fixing the volume of absolute ethanol (50 mL). Afterward, a mixed solution of $Ti(OC_4H_9)_4$ (0.34 mL) and absolute ethanol (10 mL) was added dropwise in 10 min, and the reaction was allowed to proceed for 24 h at 30 °C under continuous stirring. The resulting products were washed with ethanol, collected by centrifugation, and then dried at 110 °C for 12 h.

Synthesis of hierarchical Li_2TiO_3@$LiMn_{1/3}Ni_{1/3}Co_{1/3}O_2$ cathode material

The obtained TiO_2@$Mn_{1/3}Ni_{1/3}Co_{1/3}CO_3$ hybrid microsphere was thoroughly mixed with an appropriate amount of lithium carbonate, and the mixture was preheated at 500 °C for 8 h, and then calcined at 900 °C for 12 h in air, to form the final hierarchical Li_2TiO_3@$LiMn_{1/3}Ni_{1/3}Co_{1/3}O_2$ cathode material.

Materials characterization

The phase identification of the samples were performed with a diffractometer (D/Max-3C, Rigaku, Japan) using Cu Kα radiation (λ = 1.54178 Å) and a graphite monochromator at 36 kV, 20 mA. The scanning rate was 4° min^{-1} and the scanning range of diffraction angle (2θ) was $10° \le 2\theta \le 80°$. The morphology and atomic concentration of the samples were observed using a scanning electron microscopy (SEM) equipped with an energy-dispersive X-ray spectroscope (EDS) (JSM-6100LV, JEOL, Japan). Transmission electron microscopy (TEM, FEITecnai G2, Holland) was used to investigate the crystal structure of the materials. Surface solid-state chemistry of particles was characterized by X-ray photoelectron spectroscopy (XPS, K-Alpha 1063, Thermo Fisher Scientific, England). The chemical compositions of the resulting powders were analyzed by inductively coupled plasma (ICP) analysis.

Electrochemical test

For fabrication of the positive electrodes, the as-prepared materials were mixed with acetylene black, graphite and polyvinylidene fluoride (80:5:5:10) in N-methyl-2-pyrrolidone to obtain a slurry. The slurry was coated onto Al foil, dried and roll-pressed. The electrodes were dried overnight at 110 ℃ in a vacuum prior to use. Preliminary cell tests were done with a 2025 coin-type cell using Li metal as the anode. The electrolyte solution was a 1 M $LiPF_6$ in ethylene carbonate (EC)-dimethyl carbonate (DMC) (1:1, *v*/*v*). The cells were charged and discharged at different current densities (1 C=160 mA g^{-1}) using a Neware battery test system (Shenzhen, China) in the voltage range of 3.0-4.3 V and 3.0-4.6 V at room temperature.

Results and discussion

As revealed by scanning electron microscopy (SEM) images in Figure 1a and b, the pristine $Mn_{1/3}Ni_{1/3}Co_{1/3}CO_3$ precursor particles synthesized by co-precipitation route are spherical morphology with an average diameter of about 12 μm, and the surface of the particle is highly smooth. The atomic ratio of Ni, Co, and Mn on the surface of the pristine $Mn_{1/3}Ni_{1/3}Co_{1/3}CO_3$ precursor is 0.34:0.33:0.33 resulting from the energy-dispersive X-ray spectroscopy (EDS) analysis (Figure 1c), which is in good agreement with the designed value. The TiO_2 nano-layer has grown on the surface of spherical $Mn_{1/3}Ni_{1/3}Co_{1/3}CO_3$ precursor by controlling the hydrolysis and condensation of tetrabutyl titante ($Ti(OC_4H_9)_4$) in the ethanol/ammonia mixture. The morphology and uniformity of the TiO_2 nano-layer can be readily controlled by adjusting the volumetric ration of the ethanol/ammonia in the reaction system. When a small fraction of ammonia (< 0.2 mL) is added to the reaction system, no obvious TiO_2 nano-layer is formed on the surface of $Mn_{1/3}Ni_{1/3}Co_{1/3}CO_3$ precursor (Figure 1d-i). As the content of ammonia increases to 0.4 mL, it is apparently observed that the surfaces of particles become different from that of the pristine $Mn_{1/3}Ni_{1/3}Co1/3CO_3$, as shown in Figure 1g and k. On closer inspection, uniform and complete TiO_2 nano-layer is successful deposited on the surface of $Mn_{1/3}Ni_{1/3}Co_{1/3}CO_3$ precursor. The corresponding (EDS) spectrum in Figure 1j further confirms the presence of Ti element on the particle surface. Moreover, a cross-sectional SEM image of the TiO_2@$Mn_{1/3}Ni_{1/3}Co_{1/3}CO_3$ hybrid microsphere clearly reveals the existence of core-shell structure as expected, and the thickness of the TiO_2 outer shell

is about 60 nm (Figure S1a). The X-ray diffraction (XRD) pattern of the resulting TiO_2@$Mn_{1/3}Ni_{1/3}Co_{1/3}CO_3$ hybrid microsphere indicates that the TiO_2 shell is amorphous (Figure S2), which is ascribed to no further calcination at high temperature corresponding with previous reports.[31,32] With further increase of ammonia to 0.6 mL, uniform TiO_2 nano-layer can also be constructed on the surface of spherical $Mn_{1/3}Ni_{1/3}Co_{1/3}CO_3$ precursor (Figure 1m-o) with the thickness of around 90 nm (Figure S1b), however, isolated TiO_2 particles are formed and aggregated in the reaction system (Figure 1n). TiO_2 can't dissolve in absolute ethanol, which will result in a white suspension. When the content of ammonia is 0.6 mL, white precipitates are observed, as shown in Figure S3. It has been found from XRD results that the white precipitates are TiO_2. These results clearly indicate that the ammonia content plays an important role in controlling the reaction to grow TiO_2 nano-layer on the surface of $Mn_{1/3}Ni_{1/3}Co_{1/3}CO_3$ microsphere.

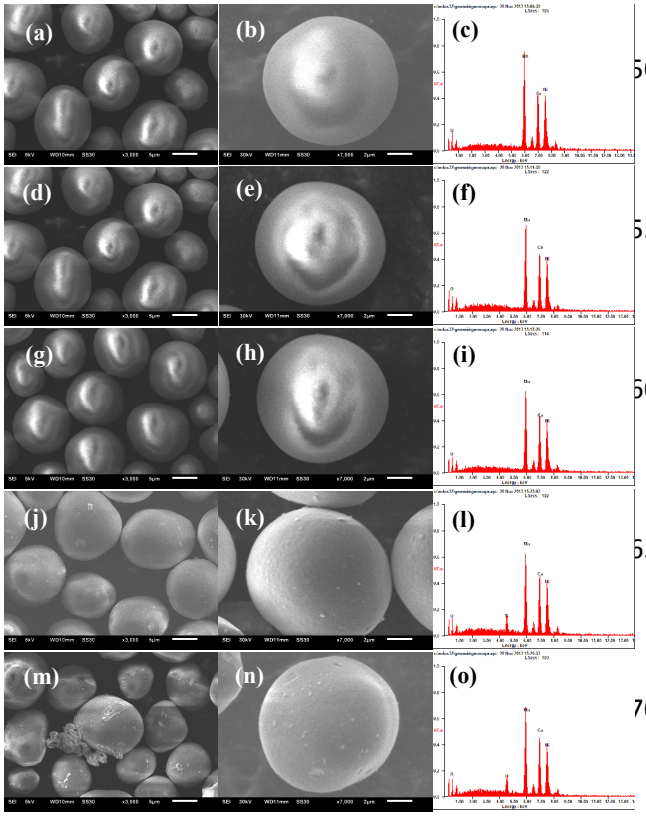

Figure 1. SEM images and corresponding EDS spectrums of the (a, b, c) pristine $Mn_{1/3}Ni_{1/3}Co_{1/3}CO_3$ and TiO_2@ $Mn_{1/3}Ni_{1/3}Co_{1/3}CO_3$ hybrid microspheres prepared with different content of ammonia: (d, e, f) 0 mL, (g, h, i) 0.2 mL, (j, k, l) 0.4 mL, (m, n, o) 0.6 mL.

The growth of the TiO_2 nano-layer on the surface of spherical $Mn_{1/3}Ni_{1/3}Co_{1/3}CO_3$ precursor can also be tuned by adjusting the reaction time and the concentration of the components. When the reaction time reduces to 12 h (the content of ammonia is 0.4 mL), incomplete TiO_2 nano-layer grows on the surface of $Mn_{1/3}Ni_{1/3}Co_{1/3}CO_3$ precursor and the thickness of TiO_2 shell becomes thinner (Figure S4a and b). Interestingly, when the reaction time lengthens to 36 h, irregular TiO_2 nano-layer is formed on the surface of the particle (Figure S4c and d). Additionally, as shown in Figure S5a and b, the $Mn_{1/3}Ni_{1/3}Co_{1/3}CO_3$ particle is coated with uniform TiO_2 shell with a thickness of ~160 nm when increasing the initial volume of tetrabutyl titante to 0.52 mL (0.4 mL ammonia, 24 h reaction time). However, once the initial volume of tetrabutyl titante reaches 1.13 mL, visible cracks can be observed for the TiO_2 shell. Meanwhile, isolated TiO_2 particle is formed and aggregated in the reaction system (Figure S5c and d). Consequently, via the hydrolysis and condensation of tetrabutyl titante ($Ti(OC_4H_9)_4$), the growth of TiO_2 nano-layer on the surface of spherical $Mn_{1/3}Ni_{1/3}Co_{1/3}CO_3$ precursor can be implemented, and importantly, the uniformity and thickness of the TiO_2 shell can be tailored by adjusting the content of concentrated ammonia, reaction time and the concentration of the components.

For the convenience of the discussion, we focus on the final liathiated cathode material obtained from the TiO_2@$Mn_{1/3}Ni_{1/3}Co_{1/3}O_2$ hybrid microshpere prepared with 0.4 mL ammonia content and 24 h reaction time (Figure 1j and k). After chemical lithiation at 900 °C for 12 h, the TiO_2@$Mn_{1/3}Ni_{1/3}Co_{1/3}CO_3$ microsphere was transformed in situ into hierarchical Li_2TiO_3@L$Mn_{1/3}Ni_{1/3}Co_{1/3}O_2$ (denoted as LTO@NCM) cathode material. The generation of Li_2TiO_3 shell is realized during the synthesis process of $LiMn_{1/3}Ni_{1/3}Co_{1/3}O_2$ active material, which is different from traditional method. In addition, the bare $LiMn_{1/3}Ni_{1/3}Co_{1/3}O_2$ (denoted as NCM) lithiated material was also prepared for comparison. The chemical composition of the hierarchical LTO@NCM was determined by inductively coupled plasma (ICP), and the molar ratio of Ti:(Ni+Co+Mn) is about 0.04:0.96. Figure 2 displays the XRD patterns of the bare NCM and hierarchical LTO@NCM materials. All the diffraction peaks of both the samples can be unambiguously indexed and assigned to the typical layered structure based on a hexagonal $NaFeO_2$ with space group of $R\bar{3}m$.[33,34] However, an enlargement of the XRD patterns over a low a small 2θ between 65° and 70° shows a slight shift to low angles for the hierarchical LTO@NCM, indicating the substitution of larger Ti^{4+} (0.605 Å) ion for smaller Co^{3+} (0.545 Å) ion and/or Mn^{4+} (0.53 Å) ion in the layered $LiMn_{1/3}Ni_{1/3}Co_{1/3}O_2$ structure.[35,36] An increase in the lattice parameters and unit cell volume for hierarchical LTO@NCM also confirms that Ti^{4+} ions infiltrate into layered structure as doping ions, as illustrated in table 1. Moreover, no obvious diffraction peaks corresponding to monoclinic Li_2TiO_3 (space group: $C/2c$) are detected in the XRD pattern (Figure 2b), which may be due to the low content of the Li_2TiO_3 outer shell.[17,37] To gain more insight into the oxidation state of transition metals in the hierarchical LTO@NCM material, X-ray photoelectron spectroscopy (XPS) measurements were performed, ant the corresponding spectra are presented in Figure 3. All of the binding energies (BEs) in the XPS analysis were corrected for specimen charging by referencing them to the C 1s peak (set at 284.6 eV). Binding energies of Ni $2p_{3/2}$ (Figure 3a), Co $2p_{3/2}$ (Figure 3b), and Mn $2p_{3/2}$ (Figure 3c) on the surface of the hierarchical LTO@NCM material are 854.5

eV, 799.8 eV, and 642.0 eV, corresponding to the predominant oxidation states of +2, +3, and +4, respectively. These results are in agreement with previous XPS results for $LiMn_{1/3}Ni_{1/3}Co_{1/3}O_2$ cathode material.[38,39] Meanwhile, the Ti $2p_{3/2}$ peak of the hierarchical LTO@NCM shown in Figure 3d is located at 457.6 eV, in accordance with Ti^{4+} oxidation state of the Li_2TiO_3 material.[40]

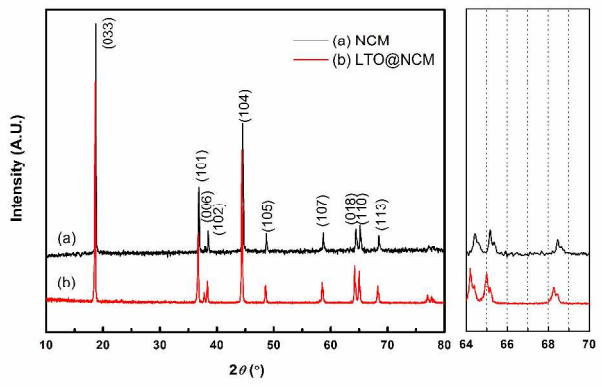

Figure 2. XRD patterns of the (a) bare NCM and (b) hierarchical LTO@NCM materials.

Table 1. Crystal cell parameters of the bare NCM and hierarchical LTO@NCM materials.

	a-Axis (Å)	*c*-Axis (Å)	Unit volume (Å^3)
NCM	2.86102	14.22607	100.85
LTO@NCM	2.86794	14.27899	101.71

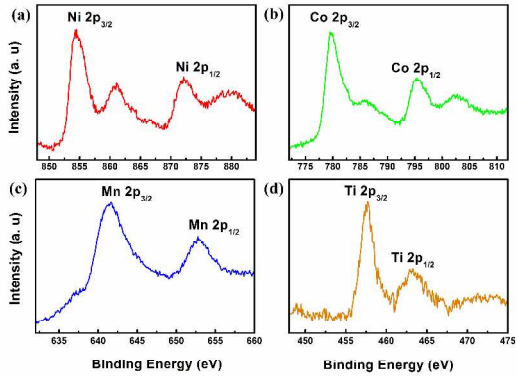

Figure 3. XPS profiles of Ni, Co, Mn, and Ti on the surface of the hierarchical LTO@NCM material.

SEM images shown in Figure 4 reveal that the as-prepared samples have a well-maintained spherical morphology in which secondary spherical particles consisted of densely aggregated submicrometer-sized primary grains. However, the hierarchical LTO@NCM particles (Figure 4c and d) seem to more compact relative to the bare NCM particles (Figure 4a and b). EDS elemental mapping of the hierarchical LTO@NCM material in Figure 4e-h show that the Ni, Co, Mn and Ti elements uniformly distribute on the surface of the particles. Transmission electron microscopy (TEM) studies provide further insights into the morphologies and detailed crystal structures of the final lithiated materials. Compared with the bare NCM (Figure 4i), TEM image of the hierarchical LTO@NCM clearly reveals the obvious core-shell structure with a uniform and tight outer shell of ~30 nm in thickness, as illustrated in Figure 4j. The shorten outer shell in final lithiated LTO@NCM material compared with that of the TiO_2@$Mn_{1/3}Ni_{1/3}Co_{1/3}CO_3$ precursor (~60 nm of the TiO_2 shell) further reveals the penetration of Ti into the bulk structure, which is consistent with the XRD results. A high-resolution (HR) TEM image (Figure 4k) of white frame region in Figure 4j obviously indicates the difference of crystal structures between the core and shell, which is also confirmed by corresponding fast Fourier transformed (FFT) patterns. Parallel lattice in the core region (region 1) corresponds to the typical layered materials with interplanar distances of 4.73 Å, which corresponds to the distance of the close packed (003) plane of the $R\bar{3}m$ layered structure. The FFT pattern of the region 1 also suggests that the crystal structure in the core is pure layered $R\bar{3}m$ phase. In addition, (002) lattice fingers with interplanar spacing of about 4.82 Å and (020) lattice fingers (~4.4 Å) can be observed in the HRTEM image in the shell (region 3) corresponds to the monoclinic Li_2TiO_3 ($C/2c$). The diffraction spots of the FFT pattern also can be indexed to (002) and (020) planes of Li_2TiO_3 phase, further suggesting a successful formation of hierarchical Li_2TiO_3@$LiMn_{1/3}Ni_{1/3}Co_{1/3}O_2$ as desired. However, the region (region 2) between the core and shell shows a mix of the two above phases. The possible reason may be due to the elements diffusion from the core to the shell and/or shell to core during the high temperature calcination, resulting in the formation of layered $Li[M_{1-x}Ti_x]O_2$ ($R\bar{3}m$) domains and/or $Li_2Ti_{1-y}M_yO_3$ ($C/2c$) (M=Mn, Ni, Co) domains in the interface between the core and shell. It is worth noting that the ionic conductivity of Li_2TiO_3 would increase when doped with foreign ions,[15] which would be more advantageous to improve the rate capability of the cathode materials.

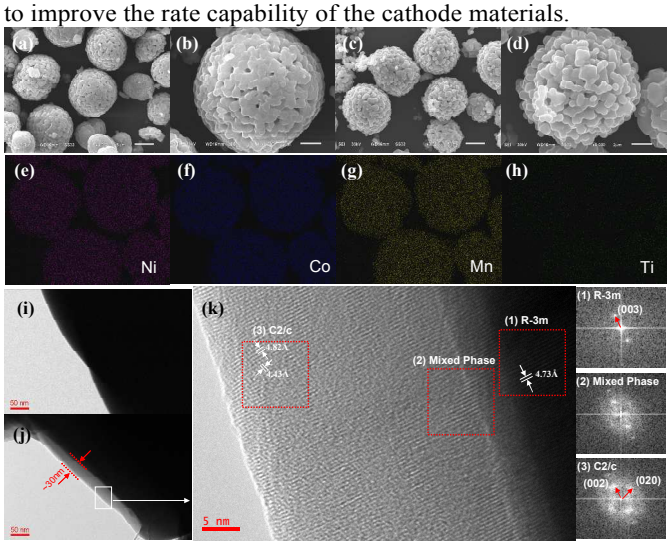

Figure 4. SEM images of the (a, b) bare NCM and (c, d) hierarchical LTO@NCM materials; (e-h) EDS elements mapping of the hierarchical LTO@NCM material; TME images of the (i) bare NCM and (j) hierarchical LTO@NCM materials; (k) HRTEM image and corresponding FFT images of white frame region in Figure 4j for the hierarchical LTO@NCM material.

As discussed above, the unique hierarchical LTO@NCM cathode material can be successfully obtained by controlling the growth of TiO_2 on the surface of $Mn_{1/3}Ni_{1/3}Co_{1/3}CO_3$ microsphere followed by a solid phase reaction. It will be interesting to study the electrochemical properties of the hierarchical LTO@NCM microsphere as cathode active material in lithium ion batteries. Figure 5a displays the initial charge/discharge profiles of the as-prepared materials in the voltage range of 3.0-4.3 V at a rate of 0.2 C (1 C=160 mAh g^{-1}). The Li/NCM cell delivers a discharge capacity of 172.4 mAh g^{-1}, while the Li/LTO@NCM cell exhibits a discharge capacity of 165.6 mAh g^{-1}. The nanosized L_2TiO_3-based shell possibly contributes to the slight reduction of the obtainable total gravimetric capacity of the hierarchical LTO@NCM material, since the L_2TiO_3 is electrochemical inactive in the voltage range of 3.0-4.3 V. However, the hierarchical LTO@NCM electrode shows inspiring improved rate capability relative to the bare NCM electrode, as illustrated in Figure 5b-d. Significantly, the hierarchical LTO@NCM electrode delivers a discharge capacity of 92.3 mAh g^{-1} even at a very high rate of 20 C, whereas only 53.6 mAh g^{-1} specific capacities can be obtained for the bare NCM electrode at the same rate. In addition, the Li/LTO@NCM cell exhibits a superior cycling stability compared with the Li/NCM cell (cycled at 10 C rate), as shown in Figure S6. Most importantly, the hierarchical LTO@NCM electrode can still deliver a high capacity of about 83.4 mAh g^{-1} after 500 cycles at a rate of 20 C (90.3 % capacity retention), as illustrated in Figure 5e-f. To our best knowledge, such high cycling performance level at high rate has been rarely reported so far.

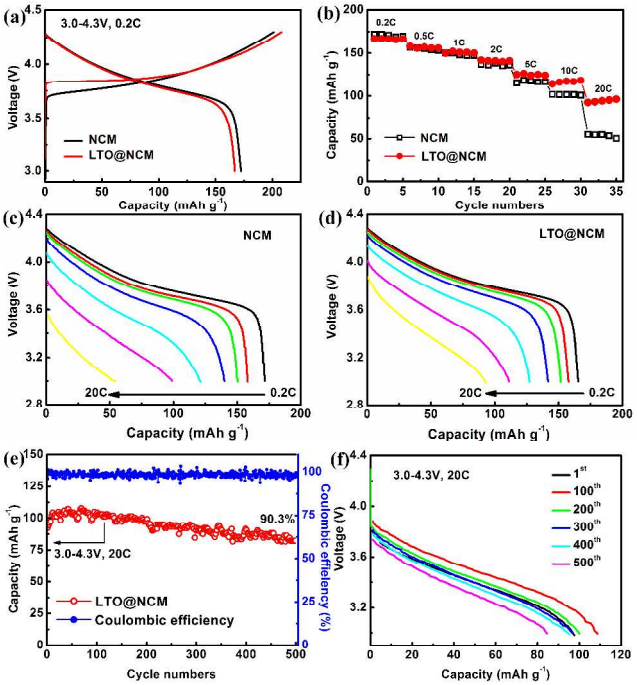

Figure 5. (a) The initial charge/discharge profiles (0.2 C), (b) rate capability and (c, d) corresponding discharge curves at different rates of the Li/NCM cell and Li/LTO@NCM cell (3.0-4.3 V); (e) cycle performance and (f) corresponding continuous discharge curves of the Li/LTO@NCM cell at a rate of 20 C.

In order to further evaluate the superiority of the hierarchical LTO@NCM material, the cells were cycled in a high voltage range of 3.0-4.6 V. Both the samples can deliver nearly 200 mAh g^{-1} capacities at 0.2 C in the voltage range of 3.0-4.6 V (Figure 6a). And yet, as shown in the Figure 6b-d, the Li/LTO@NCM cell still have a very stable capacity delivery with a capacity retention of 82.4% over 200 cycles at 1 C rate, while only 52.6% capacity retention for the Li/NCM cell.

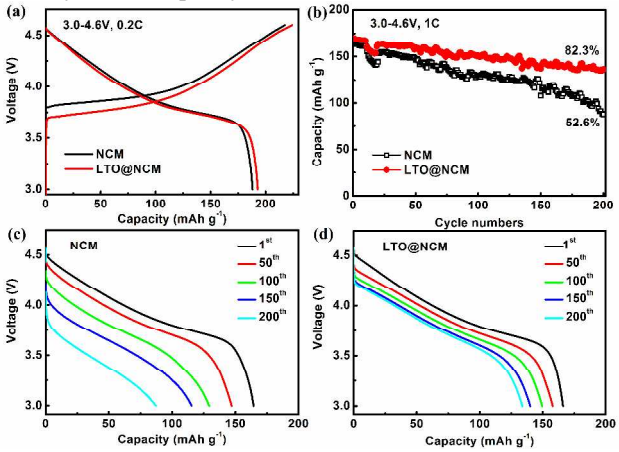

Figure 6. (a) The initial charge/discharge profiles of the Li/NCM cell and Li/LTO@NCM cell (3.0-4.6 V, 0.2 C); (b) cycle performance and (c, d) corresponding continuous discharge curves of the Li/NCM cell and Li/LTO@NCM cell at a rate of 1 C.

GITT is considered to be a reliable method to determine the diffusion coefficient of lithium ions (D_{Li}) in electrode active

materials. Assuming that lithium transport in the elelctrode obeys Fick's second law, the chemical diffusion coefficients can be obtained by the following equation:

$$D_{Li} = \frac{4}{\pi}\left(I_o \frac{V_m}{FS}\right)^2 \left(\frac{dE/dx}{dE/dt^{1/2}}\right)^2 \quad (1)$$

Where I_0 is the applied current (A), V_m is the molar volume ($cm^3\ mol^{-1}$), F is the Faraday constant and S is the surface area of the electrode (cm^2).

Figure 7a and b show the GITT curves of the NCM and hierarchical LTO@NCM during the second cycles as a function of time between 3.0 and 4.3 V. The test was performed by charge/discharge the cell for an interval of 10 min at a current density of 0.05 C, relaxing 60 min to approach nearly equilibrium state (E_s) and repeating this process. The D_{Li} of the as-prepared samples can be calculated according to the values of dE/dx (Figure 7c) and $dE/dt^{1/2}$ (Figure 7d) in Eq. (1), and the results as function of the stoichiometry x are presented in Figure 7e. It is found that the D_{Li} values of NCM are in the range from 2.75×10^{-11} to 1.32×10^{-9} $cm^2\ s^{-1}$ in the process of Li^+ extraction, corresponding to the previous report.[41] However, the D_{Li} values of LTO@NCM are in the range from 2.14×10^{-10} to 2.35×10^{-9} $cm^2\ s^{-1}$, which is obvious higher than that of NCM material. Therefore, the greatly improved electrochemical performance of the hierarchical LTO@NCM cathode material can be explained since the uniform Li_2TiO_3-based outer shell could effectively improve the lithium ion diffusion coefficient, resulting in high rate capability of the material. In addition, the complete and stable outer shell hinder the direct contact between active particles and electrolyte to reduce the side effects of the unstable Co^{4+} and Ni^{4+} with electrolyte.[15,37] Furthermore, the Ti^{4+} doping further enhances the structural stability of the layered $LiMn_{1/3}Ni_{1/3}Co_{1/3}O_2$ because of stronger binding of Ti-O compared to other M-O (M=Ni, Co, Mn) bonds.[36,42]

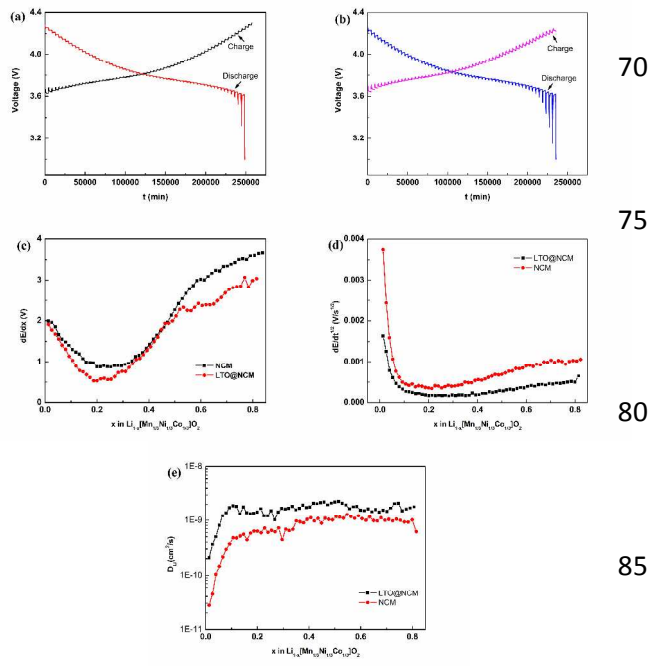

Figure 7. The GITT curves of (a) NCM and (b) LTO@NCM as a function of time between 3.0 and 4.3 V; (c) dE/dx and (d) $dE/dt^{1/2}$ as a function of the stoichiometry x; (e) the calculated D_{Li} from the GITT data for the NCM and LTO@NCM as a function of the stoichiometry x.

Conclusions

In a summary, a hierarchical Li_2TiO_3@$LiMn_{1/3}Ni_{1/3}Co_{1/3}O_2$ microsphere for advanced lithium ion battery cathode material has been prepared through a facile synthesis method. The strategy involves the growth of TiO_2 nano-layer on the surface of spherical $Mn_{1/3}Ni_{1/3}Co_{1/3}CO_3$ precursor and subsequent synchronous conversion in situ into hierarchical Li_2TiO_3@ $LiMn_{1/3}Ni_{1/3}Co_{1/3}O_2$ microsphere by solid phase reaction. The uniformity and thickness of TiO_2 shell can be easily tailed by varying the content of ammonia, reaction time and concentration of the components during Ti^{4+} hydrolysis process, which can be transitioned into uniform and robust Li_2TiO_3 coating shell. The resultant hierarchical Li_2TiO_3@ $LiMn_{1/3}Ni_{1/3}Co_{1/3}O_2$ material exhibits enhanced rate capability (92.3 mAh g^{-1} at 20 C) and excellent cyclic stability at high rate (90.3% capacity retention after 500 cycles at a rate of 20 C) and high voltage range (82.4 % capacity retention over 200 cycles in the voltage range of 3.0-4.6 V compared with the bare $LiMn_{1/3}Ni_{1/3}Co_{1/3}O_2$ material. The improved electrochemical performance is mainly attributed to the Li_2TiO_3-based outer shell, which is not only conducive to Li^+ diffusion but also can protect the host material from eroding by the electrolyte. Importantly, the strategy here could be extended to synthesize other advanced electrode materials for lithium ion batteries with rational structures and improved performances.

Acknowledgements

This work was funded by the National Natural Science Foundation of China under project No. 20871101 and 51272221, Scientific and Technical Achievement Transformation Fund of Hunan Provincial No. 2012CK1006, Key Project of Science and Technology Department of Hunan Province Government under project No. 2009WK2007, Natural Science Foundation of Hunan Province No. 12JJ5075. Colleges and Universities in Hunan Province plans to graduate research and innovation under project No. CX2012B256, Science and Technology plan Foundation of Hunan Province under project No. 2013FJ4062.

Notes and references

Key Laboratory of Environmentally Friendly Chemistry and Applications of Ministry of Education, School of Chemistry, Xiangtan University, Hunan, Xiangtan 411105, China
E-mail: wxianyou@yahoo.com, hongboshuxtu@gmail.com

Electronic Supplementary Information (ESI) available: See DOI:

1 B. C. Melot, J. M. Tarascon, *Acc. Chem. Res.* 2013, **46**, 1226.
2 X. K. Yang, D. Wang, R. Z. Yu, Y. S. Bai, H. B. Shu, L. G, H. P. Guo, Q. L. Wei, L. Liu, X. Y. Wang, *J. Mater. Chem. A*, 2014, **2**, 3899.
3 H. Li, Z. X. Wang, L. Q. Chen, X. J. Huang, *Adv. Mater.* 2009, **21**, 4593.

4 S. Lee, S. Jeong, J. Cho, *ChemSusChem* 2010, **3**, 1260.
5 T. Ohzuku, Y. Makimura, *Chemistry Letters* 2001, **30**, 642.
6 J. F. Li, S. L. Xiong, Y. R. Liu, Z. C. Ju, Y. T. Qian, *Nano Energy* 2013, **2**, 1249.
7 K.M. Shaju, G. V. S. Rao, B. V. R. Chowdari, *Electrochim. Acta* 2002, **48**, 145.
8 Z. D. Huang, X. M. Liu, S. W. Oh, B. Zhang, P. C. Ma J. K. Kim, *J. Mater. Chem.* 2011, **21**, 10777.
9 J. L. Li,C. B. Cao, X. Y. Xu, Y. Q. Zhu, R. M. Yao, *J. Mater. Chem. A* 2013, **1**, 11848.
10 Y. Wang, G. Z. Cao, *Adv. Mater.* 2008, **20**, 2251.
11 M. M. Thackeray, S. H. Kang, C. S. Johnson, J. T. Vaughey, R. Benedek, S. A. Hackney, *J. Mater. Chem.* 2007, **17**, 3112.
12 C. S. Johnson, N. C. Li, C. Lefief, J. T. Vaughey, M. M. Thackeray, *Chem. Mater.* 2008, **20**, 6095.
13 H. J. Kim, H. G. Jung, B. Scrosati, Y. K. Sun, *J. Power Sources* 2012, **203**, 115.
14 M. Gu, I. Belharouak, J. M. Zheng, H. M. Wu, J. Xiao, A. Genc, K. Amine, S. Thevuthasan, D. R. Baer, J. G. Zhang, N. D. Browning, J. Liu, C. M. Wang, *ACS Nano* 2013, **7**, 760.
15 J. S. Kim, C. S. Johnson, M. M. Thackeray, *Electrochem. Commun.* 2002, **4**, 205.
16 L. Q. Zhang, H. Noguchi, *J. Electrochem. Soc.* 2003, **150**, A601.
17 L. Q. Zhang, X. Q. Wang, H. Noguchi, M. Yoshio, K. Takada, T. Sasaki, *Electrochim. Acta* 2004, **49**, 3305.
18 X. W. Wu, Z. Y. Wen, X. G. Xu, J. D Han, *Solid State Ionics* 2008, **179** 1779.
19 X. W. Wu, Z. Y. Wen, X. Y. Wang, X. G. Xu, J. Lin, S. F. Song. *Fusion Engineering and Design* 2010, **85**, 1442.
20 L. Q. Zhang, H. Noguchi, *Electrochem. Commun.* 2002, 4, 560.
21 M. Vijayakumar, S. Kerisit,; Z. G. Yang, G. L. Graff, J. Liu,J. A. Sears, S. D. Burton, K. M. Rosso, J. Z. Hu, J. Phys. Chem. C 2009, **113**, 20108.
22 F. Wu, M. Wang, Y. F. Su, S. Chen, *J. Power Sources* 2009, **189**, 743.
23 B.C. Park, H.B. Kim, S.T. Myung, K. Amine, I. Belharouak, S. M. Lee, Y. K. Sun, *J. Power Sources* 2008, **178**, 826.
24 S. K. Hu, G. H. Cheng, M. Y. Cheng, B. J. Hwang, R. Santhanam, *J. Power Sources* 2009, **188**, 564.
25 J. H. Park, J. H. Cho, S. B. Kim, W. S. Kim, S. Y. Lee, S. Y. Lee, *J. Mater. Chem.* 2012, **22**, 12574.
26 S. T. Myung, K. S. Lee, D. W. Kim, B. Scrosati, Y. K. Sun, *Energy Environ. Sci.,* 2011, **4**, 935.
27 C. Li, H. P. Zhang, L. J. Fu, H. Liu, Y. P. Wu, E. Rahm, R. Holze, H. Q. Wu, *Electrochim. Acta* 2006, **51**, 3872.
28 Y. K. Sun, D. H. Kim, C. S. Yoon, S. T. Myung, J. Prakash, K. Amine, *Adv. Funct. Mater.* 2010, **20**, 485.
29 S. Y. Yang, X. Y. Wang, Q. Q. Chen, X. K. Yang, J. J. Li, Q. L. Wei, *J. Solid State Electrochem.* 2012, **16**, 481.
30 X. K. Yang, X. Y. Wang, G. S. Zou, L. Hu, H. B. Shu, S. Y. Yang, L. Liu, H. Hu, H. Yuan, B. A. Hu, Q. L.. Wei, L. H. Yi, *J. Power Sources* 2013, **232**, 338.
31 W. Li, F. Wang, S. S. Feng, J. X. Wang, Z. K. Sun, B. Li, Y. H. Li, J. P. Yang, A. A. Elzatahry, Y. Y. Xia, D. Y. Zhao, *J. Am. Chem. Soc.* 2013, **135**, 18300.
32 J. B. Joo, Q. Zhang, I. Lee, M. Dahl, F. Zaera, Y. D. Yin, *Adv. Funct. Mater.* 2012, **22**, 166.
33 H. B. Ren, Y. H. Huang, Y. H. Wang, Z. J. Li, P. Cai, Z. H. Peng, Y. H. Zhou, *Mate. Chem. Phys.* 2009, **117**, 41.
34 X. K. Yang, X. Y. Wang, Q. L. Wei, H. B. Shu, L. Liu, S. Y. Yang, B. A. Hu, Y. F. Song, G. S. Zou, L. Hu, L. H. Yi, *J. Mater. Chem.* 2012, **22**, 19666.
35 Z. Q. Deng, A. Manthiram, *J. Phys. Chem. C* 2011, **115**, 7097.
36 J. Shu, M. Shui, D. Xu, D. J. Wang, Y. L. Ren, J. H. Yao, R. Ma, T. F. Yi, L. F. Li, S. Gao, W. D. Zheng, L. Hou, J. J. Xu, Z. H. Zhu, M. Li, *J. Electroanal. Chem.* 2011, **663**, 90.
37 L. Q. Zhang, T. Muta, H. Noguchi, X. Q. Wang, M. J. Zhou, M. Yoshio, *J. Power Sources* 2003, **117**, 137.
38 J. Q. Deng, L. J. Xi, L. H. Wang, Z. M. Wang, C. Y. Chung, X. D. Han, H. Y. Zhou, *J. Power Sources* 2012, **217**, 491.
39 N. N. Sinha, N. Munichandraiah, *ACS Appl. Mater. Interfaces*, 2009, **1**, 1241.
40 Wagner, C. D.; Muilenberg, G. E. *Handbook of x-ray photoelectron spectroscopy: a reference book of standard data for use in x-ray photoelectron spectroscopy*; Perkin-Elmer Corp., Physical Electronics Division: 1979.
41 K. M. Shaju, G. V. Subba Rao, B. V. R. Chowdari, *Journal of The Electrochemical Society*, 2004, **151**, A1324.
42 H. S. Liu, J. Li, Z. R. Zhang, Z. L. Gong, Y. Yang, *Electrochim. Acta* 2004, **49**, 1151.

The Table of Contents entry

Graphic:

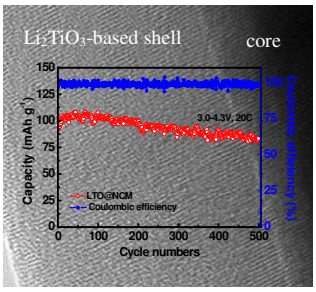

Text: $LiMn_{1/3}Ni_{1/3}Co_{1/3}O_2$ microsphere covered by nanosized Li_2TiO_3-based shell shows high rate capability and excellent cycling performance as cathode material.